JCTC Journal of Chemical Theory and Computation

Understanding Rubredoxin Redox Potentials: Role of H-Bonds on Model Complexes

Ana Patricia Gámiz-Hernández, Artur S. Galstyan, and Ernst-Walter Knapp*

Institute of Chemistry and Biochemistry, Department of Biology, Chemistry, and Pharmacy, Freie Universität Berlin, Fabeckstrasse 36a, D-14195 Berlin, Germany

Received June 29, 2009

Abstract: The energetics of redox states in different models of rubredoxin-like iron−sulfur complexes (ISC) was computed using a combination of density functional and electrostatic continuum theories. In agreement with experiment, the calculated redox potential for the small ISC model $[Fe(SCH_2CH_3)_4]^{1-,2-}$ in acetonitrile was −813 mV [Galstyan, A. S.; Knapp, E. W. *J. Comput. Chem.* **2009**, *30*, 203−211] as compared to the measured value of −838 mV. Surprisingly the experimental values for rubredoxin (Rd) are much higher ranging between −87 and +39 mV. These large variations in redox potentials of ISC models and ISC in Rd are due to specific conformational symmetries adopted by the ligands due to both the protein environment and type and the number of H-bonds, and the dielectric environment. In a dielectric environment corresponding to proteins ($\varepsilon = 20$), the computed ISC redox potentials shift positive by about 64 mV for Fe−S···H−N and 95 mV for Fe−S···H−O H-bonds, correlating well with data estimated from experiments on ISC proteins. In aqueous solutions ($\varepsilon = 80$), a positive shift of 58 mV was computed for Fe−S···H−O H-bonds (using a model with the same ISC conformation as in Rd) in agreement with a measured value for Rd with partially solvent exposed ISC. The latter demonstrates the dependence of the ISC redox potentials on the environment (solvent or protein). For a model whose chemical composition is analog to the relevant part of ISC in a specific Rd, the computed redox potential of the model agrees with the measured value in Rd. This study allows to understand redox potential shifts for small ISC models and ISC in proteins.

Introduction

Iron−sulfur complexes (ISC) are common redox-active cofactors in proteins.[2−6] These ISC proteins mediate electron transfer processes occurring in enzymatic catalysis, photosynthesis and respiration. ISC proteins are ubiquitous in nature and despite their similarity in physicochemical composition and structure of the iron sulfur complexes their redox potential values in proteins cover a large interval extending from −700 to +400 mV.[3,7−10] Interestingly, the measured redox potential of the most elementary ISC model $[Fe(SCH_2CH_3)_4]^{1-,2-}$ in acetonitrile (AN) is with −838 mV even lower.[11] This large variation in the ISC redox potentials was suggested to be due to differences in solvation,[12−15] H-bond pattern[9,16−21] and the electrostatic environment of the redox centers provided by the protein.

There are two types of H-bonds commonly formed by ISC with ligating groups of the protein: Fe−S···H−N and Fe−S···H−O. The first type arises mainly from peptide backbone interactions with the ISC, while the second type is generally due to interactions with amino acid side chains of serine and tyrosine. Analysis of ISC models and ISC with peptide-based ligands involving Fe−S···H−N H-bonds[22−28] analogue to rubredoxin (Rd) and ISC in proteins[16,18,29−33] demonstrated that the redox potentials are shifted positively in the presence of H-bonds with sulfur. The influence of Fe−S···H−O H-bonds on the ISC redox potentials was quantified through mutations in corresponding proteins yielding a positive shift in Rd (65 mV for Ala to Ser mutation)[34] and Rieske proteins (44 or 65 mV for Tyr to Phe and −95 or −120 mV for Ser to Ala mutations).[35,36]

* Corresponding author: Fax: +493083856921. E-mail knapp@chemie.fu-berlin.de.

10.1021/ct900328c CCC: $40.75
Published on Web 09/16/2009

To study the influence of Fe−S···H−N H-bonds in proteins is more difficult, since these interactions involve backbone nitrogen atoms that cannot be removed without distorting the protein structure significantly. Hunsicker-Wang[18] analyzed the measured redox potential shifts of Rieske and Rieske-type proteins with different H-bond patterns leading to estimates of 70 mV for Fe−S···H−N and 140 mV for Fe−S···H−O. An analogue analysis is not possible for Rd, since the six amide H-bonds are present in all known Rd crystal structures. In this case, the influence of H-bonds on Rd redox potentials was studied by site-directed mutagenesis, which varied the redox potential, modifying the strength but not the number of H-bonds with the ISC.[29−31,33,37] Unfortunately, these series of mutations involve also changes in the dielectric environment and have side effects in protein conformation,[10,34,38] making it difficult to extract the influence of Fe−S···H−N H-bonds on the Rd redox potentials faithfully.

Theoretical results on ISC[39−41] and Rd[9,42−45] redox potentials obtained with quantum chemical and electrostatic energy computations demonstrated the difficulty to predict small variations (100 mV) in redox potentials and the limitations using continuum dielectric models to reproduce and understand properties of ISC in different environments. In the protein, specific H-bonds may help to delocalize and stabilize excess negative charges, which may particularly occur for ISC in a reduced state. Hence, to describe ISC redox potentials of model compounds and in proteins, H-bonds with the ISC sulfur atoms should be considered explicitly.[39,40]

Recently, electrostatic energy computations were combined with density functional theory (DFT) using a new functional B4(XQ3)LYP to evaluate accurate redox potentials of transition metal complexes in different solvents.[1] This method is able to predict experimental redox potentials of mononuclear transition metal (Fe, Ni, Mn) complexes in different solvents (water, AN, and dimethylformamide) with nearly 60 mV absolute value accuracy and is, therefore, an ideal tool to investigate how ISC redox potentials vary with different H-bond patterns. Similar accuracy was achieved earlier[46] for the redox potential calculations on the small organic compounds using the much more expensive ab initio G3MP2-method[47] combined with independent electrostatic computations.

In order to avoid the complications of ferromagnetic coupling observed in multinuclear ISC,[39,48−52] we have chosen the ISC of Rd that is one of the smallest redox-active proteins, containing the simplest ISC consisting of one iron coordinated by sulfur atoms of four cysteines. There are several crystal structures of Rd available (Figure 1a, for references see Supporting Information, Table S1.1).

The simplicity of ISC in Rd made it possible to construct several Rd-like ISC models where one can vary conformations and H-bond numbers and types and construct large models that include all structural elements to reproduce measured redox potentials of ISC models and Rd. In this study, model **4**, described later in detail, (Figure 1b) is most similar to the ISC in Rd. Therefore, it can best be used to study the dependence of Rd redox potentials on various details of the protein structure.

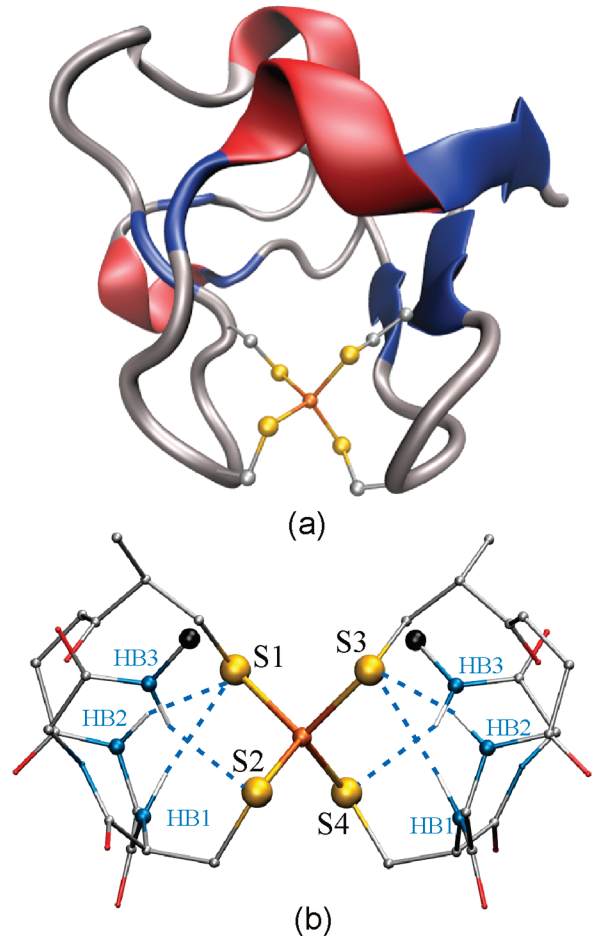

Figure 1. (a) The ISC in Rd is formed by one iron ligated by four Cys residues. The ISC in Rd interacts with the protein backbone through six amide H-bonds that are described by model **4** [depicted in part (b)], which mimics the three H-bond types (HB1, HB2, HB3) found in Rd without the sequence specific amino acid side chains. For a definition of the H-bond types, see Scheme 1 and text. It is the most detailed model to study the ISC in Rd. The redox potential calculated for this model in a dielectric continuum of $\varepsilon = 20$, corresponding to a protein environment, is +57 mV, which is close to values measured in different Rds (−87 to +39 mV). The color code of atoms corresponds to conventional CPK. We denoted in black color the two C-atoms, where model **4** was truncated from the ISC embedded in Rd.

In this study we report on computed ISC redox potentials obtained with a combination of DFT and electrostatics[1,54] to estimate the effect of the two different H-bond partners (Fe−S···H−N and Fe−S···H−O) in ISC models and proteins. In agreement with experiments in proteins,[18,33−36] our computed ISC redox potentials are shifted positive by H-bonds to sulfur with a smaller influence for Fe−S···H−N than for Fe−S···H−O H-bonds due to the lower polarity of the NH versus the OH groups. We also found a linear correlation between the number of H-bonds and the ISC redox potential shift in agreement with experimental observations.[18] Another important effect influencing ISC redox potentials found in our computations is the closeness of the solvent (degree of solvent exposure) to the iron−sulfur core,

Scheme 1. The H-bonds of the ISC in *Clostridium pasterianum* (*Cp*) Rd (PDB code 1IRO[53]) Formed with the Protein Backbone NH-Groups Are Displayed[a]

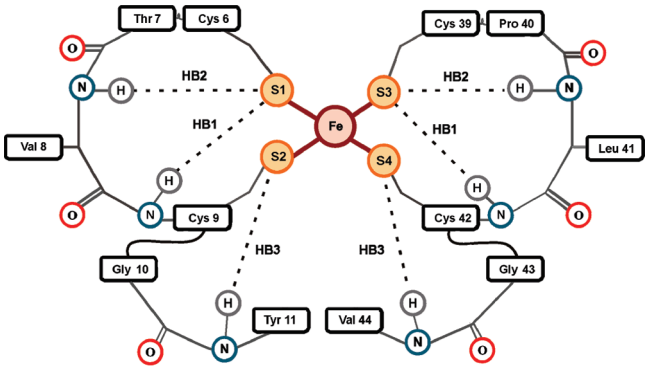

[a] There are six amide H-bonds of three different types related by two-fold rotation symmetry (C_2). Each H-bond type possesses different orientation and flexibility that affects the electronic state of the ISC model. The H-bonds of type HB1, HB2, and HB3 involve the residue pairs Cys9/Cys42, Val8/Leu41, and Tyr11/Val44, respectively. The two symmetry-related sulfurs from Cys6 and Cys39 are simultaneously involved in H-bonds of types HB1 and HB2, while the two sulfurs from Cys9 and Cys42 form only a single H-bond of type HB3. Further explanation of the H-bond types is given in the text. In Rd, the orientations of Cys6 and Cys9 lead to C_2-symmetry in contrast to the S_4-symmetry observed in small ISC models. The backbones of Cys6 and Cys39 are buried in the protein, while the backbones of Val8/Cys9/Tyr11 and Leu41/Cys42/Val44 are solvent exposed.

which varies with the size of the ISC model. These findings are relevant for ISC proteins where we observed a strong dependence of the ISC redox potential with the dielectric environment,[14,15] which combined with H-bond effects provide the key to understand the variation of the redox potentials for different ISC models and ISC in proteins.

Materials and Methods

ISC H-Bonds in Rd. The ISC redox potentials in Rd are affected by the strength of the six amide H-bonds formed with the protein backbone.[16,29−33] We distinguish three types of H-bonds (Figure 1a) (HB1, HB2, HB3, depicted in Scheme 1). Each of the ISC sulfur atoms, S1 and S3, is engaged in two H-bonds, which we call type HB1 and HB2. The two HB1 are formed between the NH-groups of the other two Cys ligating to the iron with sulfur atoms S2 and S4. The two HB2 are formed with the NH-groups of the residues next to these Cys in the N-terminal direction. The ISC sulfur atoms S2 and S4 are involved in single H-bonds each, called type HB3. These H-bonds are formed with the amide backbone of the residues two positions in the C-terminal direction from the ligating Cys providing the sulfur involved in this H-bond. The amide groups forming HB1 are more constrained than that of HB2 and HB3, since they belong to the backbone of the ligating Cys.

H-bonds of Rd-like ISCs. Model **1a** with redox states $[Fe(SEt)_4]^{1-/2-}$ is the most simple Rd-like ISC (Figure 2). Its initial coordinates were taken from a synthetic ISC models[55] of known crystal structure [Cambridge structural database (CSD) reference code CANDAW] possessing a nearly ideal S_4-symmetry. Model **2a** has the same chemical

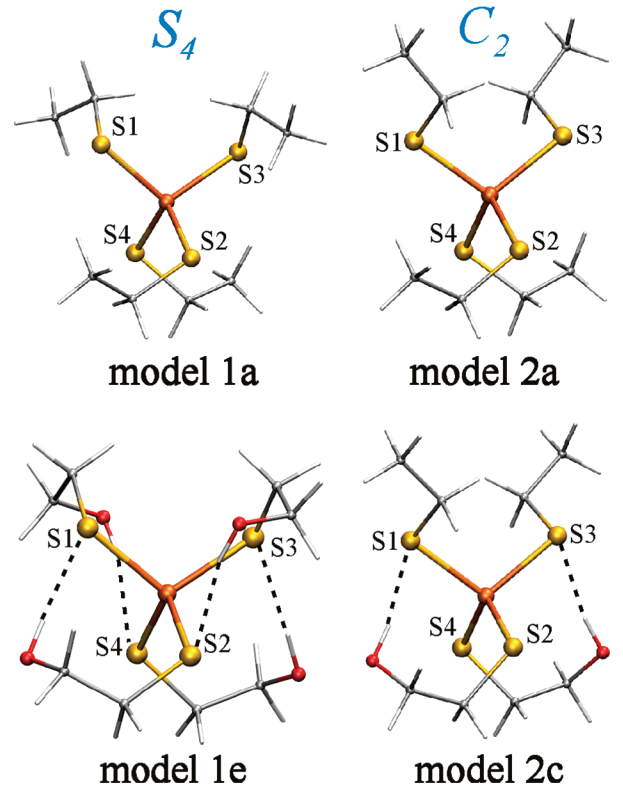

Figure 2. ISC models with symmetry S_4 and C_2 (models **1a** and **2a**, respectively) and ISC models **1e** and **2c** with Fe−S···H−O H-bonds derived from models **1a** and **2a**, respectively. The H-bond models **1b**−**e** and **2b**−**c** were constructed from model **1a** and **2a**, respectively, by substituting the corresponding terminal $-CH_3$ groups by $-CH_2OH$ groups, which form intramolecular H-bonds with the sulfur atoms and preserve the same solvation surface to account for the redox potential shift dependence on the number of H-bonds. Due to symmetry, model **1a** allows formation of a maximum four H-bonds (model **1e**), while in model **2a** just two H-bonds are possible (model **2c**).

composition as model **1a** but was built in order to represent a conformation closer to the one found in Rd crystal structures, where the ISC possesses a distorted C_2-symmetry due to steric constrains.[56] The initial geometry of model **2a** is based on the coordinates of the $Fe(Cys)_4$ complex from *Clostridium pasterianum* (*Cp*) Rd (PDB code 1IRO[53]), where the backbone of each Cys was substituted by a methyl group resulting in sulfur with an ethyl group (Figure 2). The use of ISC with ethyl groups was recommended by Szilagy and Winslow,[57] to avoid the spread of negative charge in the H-atoms observed in ISC models with methyl groups.[33,39,50,58] Models **1a** and **2a** were subsequently used to model systematically ISCs with a different H-bond pattern, replacing the terminal $-CH_3$ groups of the ligands by one to four $-CH_2OH$ groups in model **1a** or one to two $-CH_2OH$ groups in model **2a** to form intramolecular S···H−O H-bonds yielding models **1b**−**e** and **2b**−**c** with S_4- and C_2-based symmetry, respectively (listed in Table 3). ISC model complexes with S···H−O H-bonds were built to mimic the interaction of a Ser side chain with ISC observed in several ISC proteins.[18,34,59] Due to the C_2-symmetry of model **2a**, it was only possible to consider ISCs with one and two S···H−O H-bonds.

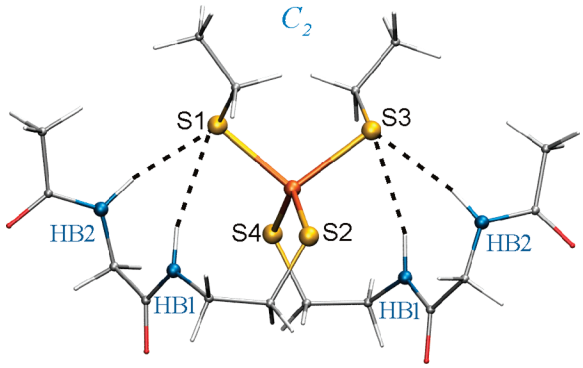

Figure 3. ISC model **3a** with four amide H-bonds (two HB1 and two HB2, as defined in Scheme 1). ISC models related to model **3a** but with a smaller number of H-bonds [models **3b**−**h**] were obtained by substituting one (**3b**, **3c**), two (**3d**, **3e**), three (**3f**, **3g**), or all four NH-groups by CH_2-groups. Thus, the solvent boundaries of the ISC models are approximately preserved. This avoids influences from different electrostatic boundaries on the ISC redox potentials and allows to observe how the redox potential shifts with the number of H-bonds.

Model **3a** (Figure 3) possesses four H-bonds with NH-groups two of type HB1 and two of type HB2 reflecting part of the H-bond pattern of the ISC in Rd (see Scheme 1). The coordinates of this model were generated based on the crystal structure of *Cp* Rd.[53] Models **3b**−**h** were derived from model **3a** by substituting one (**3b, 3c**), two (**3d, 3e**), three (**3f, 3g**), or four (**3h**) of the NH-groups by CH_2-groups to reduce the number of H-bonds accordingly.

Model **4** (Figure 1b) includes all six amide H-bonds formed with the protein backbone as in Rd (Scheme 1). The coordinates of this model were modeled based on the crystal structure of *Cp* Rd.[53] For the backbone parts of the ISC model **4,** which are not engaged in H-bonds with sulfur and not relevant for this study, we substituted −N−H and −C═O groups by $-CH_2$ groups without distorting the remaining backbone conformation. This, relatively large ISC model, is a trade-off between the limitations imposed by the performance of quantum chemical computations and the sufficiently faithful modeling of the ISC protein environment. Nevertheless, it can account for three main factors that shift the redox potential in ISC: ISC symmetry, H-bonds, and dielectric environment.

Redox Potentials. Absolute values of the ISC redox potentials were calculated using the B4(XQ3)LYP approach,[1] which employs the DFT method with a modified functional combined with a postcomputational charge dependent empirical DFT correction and subsequent optimized electrostatics to compute solvation energies. In the B4(XQ3)LYP approach, we compute the free energy difference of reduced minus oxidized state in vacuum ΔG_g°, combining quantum chemical DFT-based ($G_g^{\circ,\,\mathrm{B4LYP}}$) and empirical ($G_X$) contributions as follows:

$$\Delta G_g^\circ = \Delta E_0^{\mathrm{B4LYP}} + \Delta\mathrm{ZPE} + \Delta G_{0\rightarrow 298\mathrm{K}} + \Delta G_X(q_{\mathrm{red}}) = \Delta G_g^{\circ,\mathrm{B4LYP}} + \Delta G_X(q_{\mathrm{red}}) \quad (1)$$

with the empirical term ΔG_X (in units of kcal·mol^{-1}), depending on the total charge q_{red} of the reduced state, where $\Delta G_X(q_{\mathrm{red}}) = G_X(q_{\mathrm{red}}) - G_X(q_{\mathrm{red}} + 1)$ and

$$G_X(q) = -0.333q^3 + 1.545q^2 + 21.634q \quad (2)$$

The B4LYP functional contains the same terms as the B3LYP but with weights that differ for the exact exchange. The weight parameters for the two exchange terms in the B4LYP functional are decoupled. While the parameter for the local exchange remains at the B3LYP value of 0.80, the exact exchange term is reduced from 0.20 to 0.12, and the other parameters are the same as in the B3LYP functional.[1] An empirical correction G_X compensates for the energy deficit caused by the decrease of the exact exchange contribution and is fitted after the SCF computation to reproduce correctly the experimental redox potentials.[1]

The quantum chemical ground-state electronic energies (E_0^{B4LYP}) are computed in vacuum for both the oxidized and reduced states using the incomplete DFT functional B4LYP,[1] while the zero-point vibrational energies for the vibrational ground state (ZPE) and the free energies for the thermal excited states at 298 K ($G_{0\rightarrow 298\ \mathrm{K}}$) are calculated with the standard B3LYP functional according to the previous work.[1]

The free energy of a redox reaction in solution ΔG_s° can be computed as

$$\Delta G_s^\circ = \Delta G_g^\circ + \Delta\Delta G_{\mathrm{sol}}^\circ \quad (3)$$

where $\Delta G_g^\circ$and $\Delta\Delta G_{\mathrm{sol}}^\circ$ are, respectively, the differences of vacuum and solvation energies between the reduced and oxidized states.

The standard (°) redox potential E° of the redox reaction $\mathrm{Ox_s} + \mathrm{e_g} \rightarrow \mathrm{Red_s}$ in solution relative to the absolute potential of the standard hydrogen electrode (SHE), E_{SHE}°, is given by

$$E^\circ = E_{\mathrm{SHE}}^\circ - \frac{\Delta G_s^\circ}{nF} \quad (4)$$

where $F = 23.06$ kcal·mol^{-1} V^{-1} is the Faraday constant and n is the number of transferred electrons (in our case $n = 1$).

For the E_{SHE}°, the values of 4.43,[61] 4.44,[62] and 4.36[63] are known. Since the value of the free energy of hydration, included in the calculation of E_{SHE}° stems from the indirect measurements, their accuracy will influence the value of E_{SHE}°. The value of −4.36 eV for E_{SHE}° has been suggested recently,[63] based on the newest results of proton hydration energy from gas-phase experiments.[64] However, the exact value of E_{SHE}° is not crucial in our method, since the computed redox potentials can be easily adjusted to another value of E_{SHE}°. Here, we use −4.44 V,[62] as recommended by IUPAC.

Quantum Chemical Computations. Quantum chemical calculations were performed using DFT. Geometries of all considered ISC models were optimized in vacuum using the B3LYP[65−69] functional with LACVP[70] effective core potential for the iron atom and the 6-31G** basis functions for main-group atoms (LACVP**). Single-point electronic energies E_0^{B4LYP} needed for the computation of absolute redox potentials of the model complexes within the B4(XQ3)LYP approach[1] were calculated for optimized geometries using the incomplete functional B4LYP[1] with the basis sets LACV3P**++, including the LACV3P[71] effective core potential for the iron atom and the 6-311++G** basis

function for all other atoms. Vibrational frequency calculations were done using the B3LYP functional with LACVP** basis set without rescaling of vibrational frequencies. Since the ISCs in Rd are in the high spin state,[72] the model compounds with total spins $S = 5/2$ and $S = 2$ for reduced and oxidized forms, respectively, were considered. All quantum chemical computations were performed by the program Jaguar 5.5.[71]

Atomic Partial Charges. Atomic partial charges of the ISC were obtained from electrostatic potentials using the restraint electrostatic potential (RESP) method.[73,74] The electrostatic potentials were calculated quantum chemically in vacuum at the B3LYP/LACVP** level using Jaguar 5.5.[71] The atomic partial charges were determined in two stages, using hyperbolic restraints with the total charge fixed. In the first stage of the RESP procedure, the atomic charges were allowed to change with a restraining weight of 0.0005 au. In the second stage, the charges on C- and H-atoms were left free, while all other atomic charges were constrained at their values obtained from the first stage, using a restraining weight of 0.001 au.

Solvation Energy. For the computation of solvation energies ΔG°_{sol}, the environment was represented as a dielectric continuum. For water, a high dielectric constant ($\varepsilon_W = 80.0$) was used, while for AN a lower dielectric constant ($\varepsilon_{AN} = 37.5$) was used. The value of the dielectric constant appropriate to describe proteins depends on the atomic detail of the protein model[75,76] and the method used to represent the continuum[77] and can vary typically between 4 and 30. For protein models with all atomic details, $\varepsilon_P = 4$ is generally used.[78] For implicit protein models with no atomic detail, the appropriate dielectric constant varies typically between 10 and 30. For the sake of simplicity, we consider in this application an implicit protein model with no explicit atom representation assuming $\varepsilon_P = 20$.

The solvation energies were computed with the program module "solvate" from the MEAD program suite.[79,80] The dielectric constant within the solute cavity was taken to be $\varepsilon = 1$. The solute cavity was defined by the joint van der Waals volumes of all atoms using atomic radii, as in a previous work.[1] Since H-atoms have the ability to approach other atoms most closely, they will have the strongest electrostatic interactions with other atoms, if they are polar. To account for this effect, we use larger atomic radii for solute atoms in aprotic solvents, like AN, than in protic solvents, since in protic solvents polar hydrogens are absent.[46] Outside the solute cavity, the dielectric constant appropriate for the solvent/protein was taken, and the ionic strength was set to zero. As for the solvent probe radius, we used 1.4 Å for water and molecular groups from the protein environment, while we used 2.23 Å for AN.[1] A two-step focusing procedure was used to solve the Poisson equation numerically on a grid consisting of $(189)^3$ points, using first a low- and then a high-resolution grid with lattice constants of 0.4 and 0.1 Å, respectively.

Results and Discussion

The shifts of redox potentials of our ISC models depend basically on the following factors: the change of symmetry of the ISC (from S_4 to C_2) and the number and type of H-bond partners (Fe−S···H−O or Fe−S···H−N) interacting with sulfur ligated to iron and dielectric environment (degree of solvent exposure).[12−19] These factors are presented and discussed in detail in the following sections. We start with the symmetry effect, discussing also how it affects the charge distribution. Then we analyze the influence of the H-bond partners for different numbers and types of H-bonds. Finally, with a model similar to ISC in rubredoxin (Figure 1b), we quantify the factors shifting the redox potential from the ISC models to protein.

ISC Models with S_4 and C_2 Symmetry. Geometry comparison of an ISC model with similar composition but different conformational symmetry of the ligands (model **1a** with S_4 and model **2a** with C_2 symmetry, Figure 2) shows that the ISC core structure consisting of $Fe(SC)_4$ is nearly invariant (see Supporting Information, Table S3.1). Structural differences appear in the dihedral angles Fe−S−C−C involving the ethyl groups, which in the oxidized state are at 8° for Fe−S1−C−C and Fe−S3−C−C and at −8° for Fe−S2−C−C and Fe−S4−C−C with S_4 symmetry, while in the model with C_2 symmetry the corresponding values are 17° and 85°, respectively (see Figure 2).

The atomic partial charges of the iron and sulfur atoms of models **1a** and **2a** essentially do not depend on symmetry, while the charges of the attached ethyl groups do depend on symmetry (Supporting Information, Table S4.1). The groups (S2/S4)−CH_2−CH_3 of model **1a** carry larger dipole moments than the corresponding atoms of model **2a** with C_2 symmetry.

Table 1 shows the energies of the most elementary ISC models **1a** and **2a** with S_4 and C_2 symmetry, respectively. The energies are given in kcal/mol relative to the vacuum oxidized state in S_4 symmetry (whose energy was set to zero) using the conventional B3LYP DFT functional as well as the alternative approach with the B4(XQ3)LYP DFT functional and subsequent post-SCF correction.[1] Comparing the vacuum energies, we recognize that the ISC model in the oxidized state is more stable in the S_4 than in the C_2 symmetry for both DFT functionals, while this is opposite for the reduced state. This behavior changes in the condensed phase where, according to our computations, the S_4 symmetry conformer is more stable in both redox states (valid for environments with $\varepsilon > 10$). We have tested this behavior for both water and acetonitrile. In Table 1 we show the energies for the dielectric constant of $\varepsilon = 37.5$, corresponding to acetonitrile but used the small set of atomic radii suitable of protic solvents, while AN is an aprotic solvent. This setting is close to the electrostatics prevailing in the protein environment with an effective dielectric constant of $\varepsilon = 20$, where we also verified that the S_4 conformer (model **1a**) is more stable than the C_2 conformer (model **2a**) in both redox states. Hence, the fact that in the protein the ISC possesses C_2 symmetry is due to the constraints, which the protein applies to the ISC ligand geometries.

Table 2 shows the redox potentials of models **1a** and **2a.** The calculated redox potential of model **1a** in AN is −813 mV,[1] which is in agreement with the measured value of −838 mV.[11] This very negative redox potential demonstrates the

Table 1. Computed Energies (kcal/mol) of the ISC Models **1a** and **2a** (Figure 2) Relative to the Oxidized States in Vacuum Using the DFT Approach with Functionals B3LYP and B4(XQ3)LYP[1] and Symmetries S_4 and C_2

	symmetries			
ISC models	S_4[a]	C_2[b]	S_4[a]	C_2[b]
Energies in Vacuum, ΔG_g° (eq 1)				
	B3LYP		B4(XQ3)LYP[1]	
$[Fe(SCH_2CH_3)_4]^{1-}$	0.00[c]	3.40	0.00[c]	3.63
$[Fe(SCH_2CH_3)_4]^{2-}$	31.54	28.92	29.09	26.61
Energies in Acetonitrile[d] ΔG_s° (eq 3)				
	B3LYP		B4(XQ3)LYP	
$[Fe(SCH_2CH_3)_4]^{1-}$	−44.33	−39.55	−44.33	−39.32
$[Fe(SCH_2CH_3)_4]^{2-}$	−126.31	−125.52	−128.75	−127.82

[a] Model **1a**. [b] Model **2a** (see Figure 2). [c] To facilitate comparison of energies for different redox states and symmetries, the energy of the oxidized state in symmetry S_4 was set to zero. [d] $\varepsilon = 37.5$ corresponds to AN, but with smaller solute atomic radii it corresponds to protic solvent environment like water or protein.

discrepancies in redox potentials between the small model compounds in aprotic solvents and the redox potentials reported in Rd, which is between −87 and 39 mV (see Supporting Information, Table S1). Changing the solvent from AN to water stabilizes the reduced state of model **1a** (S_4 symmetry), shifting the redox potential by a large positive value of 798 mV as observed in experiments of ISC measured in aprotic and aqueous solutions.[22,23] To demonstrate this effect more clearly, we computed the redox potential of ISC in a dielectric corresponding to AN but assumed that AN is a protic solvent where the small solute atomic radii apply. Assuming such an artificial solvent condition, the redox potentials of the ISC are computed to be −104 and −28 mV for S_4 (model 1**a**) and C_2 (model 2**a**) symmetry, respectively. This is an enormously large shift to more positive redox potentials as compared to the conditions appropriate for the aprotic solvent AN. These large shifts are due to the smaller solute atomic radii, which are applicable for protic dielectric environments of water and protein as compared to AN. In an environment of a large dielectric constant, smaller solute atomic radii lead implicitly to strong H-bonds, formed with the electronegative atoms of the solute.

In our study of Rd-like ISCs, we observed that the change of conformational symmetry of the ISC (from S_4 to C_2) is also up-shifting the redox potential. Due to structural peculiarities, the free energy differences (ΔG_g° and $\Delta\Delta G_{sol}^\circ$, see eq 2) between the reduced and oxidized states are larger in the conformation with S_4 than with C_2 symmetry. This leads to an increase of the $[Fe(SCH_2CH_3)_4]^{1-/2-}$ redox potential by 71 mV in water and 211 mV in AN when changing the symmetry from S_4 to C_2 (Table 2). To analyze the symmetry related redox potential shifts more in detail, we computed the ISC redox potentials of model **1a** in water using the coordinates of S_4 symmetry combined with atomic partial charges of C_2 symmetry and vice versa yielding redox potentials of −142 and −273 mV, respectively. Comparing these values with the computed redox potentials combining coordinates and charges appropriately (Table 2), we observe a down-shift of the redox potentials for the artificial combinations of coordinates and charges, which is much stronger for C_2 than for S_4 symmetry. Interestingly, changes in the charges and the coordinates shift the redox potentials in opposite directions such that the net effect in water is a moderate upshift of the ISC redox potential going from S_4 to C_2 symmetry. However, in AN, this upshift is considerably larger at about +200 mV. Hence, the variation in ISC redox potentials with symmetry clearly shows that redox potentials in Rd can be better understood, if the ISC models considered possess the same symmetry as in the protein.[56]

Table 2. Computed Free Energy Differences and Comparison of Calculated and Measured Redox Potentials of the ISC Model $[Fe(SCH_2CH_3)_4]^{1-/2-}$ in Two Different Symmetry States, S_4 (model **1a**) and C_2 (model **2b**)

	E_{comp}° (eq 4), mV			E_{exp}°, mV
ISC models	water[a]	AN[a] protic	AN[b] aprotic	AN
$[Fe(SCH_2CH_3)_4]^{1-/2-}$ (S_4)	−15	−104	−813[c]	−838[d]
$[Fe(SCH_2CH_3)_4]^{1-/2-}$ (C_2)	56	−28	−602	−

[a] Inside the ISC volume, the dielectric constant is unity, while outside we used 80 for water and 37.5 for acetonitrile (AN). Here, we use the same smaller solute atomic radii for AN as for water, corresponding to a protic rather than an aprotic solvent. [b] In this case we use the larger solute atomic radii corresponding to AN. [c] Ref 1. [d] Ref 11.

ISC Models with Fe−S···H−O H-Bonds. The considered ISC models with different H-bond geometries of type Fe−S···H−O are presented in Table 3. The ISC models **1**(**b**−**e**) and **2**(**b**−**c**) are variations of models **1a** and **2a**, respectively, which involve OH groups that form H-bonds with sulfur. The OH group H-bond partner is not present in native Rd but was created for a mutant of *Pyrococcus abyssi* (*Pa*)[34] to measure the influence of S···H−O H-bond in Rd. The crystal structure of the *Pa* mutant was solved at high resolution (0.86 Å), and the redox potential was estimated to shift by 65 mV due to the Fe−S···H−O H-bond.[34] In this crystal structure, the S···O distance is 3.24 Å, and the S···H−O angle with the H-bond partner is 158.7°. The geometry optimized structures of our ISC models yield in the oxidized state S···O distances varying from 3.26 to 3.58 Å and H-bond angles in the range 164.3 to 178.6°. Hence, our calculated S···O distances in the ISC models (Supporting Information, Table S3.3) seem to agree with the value obtained from the Rd crystal structure, although, the calculated H-bond angles are closer to linearity than in the crystal structure. The latter is actually the reason that the S···O distance in the crystal is smaller than the average distance obtained with the ISC models.

In proteins, the S···O distances of H-bonds between OH groups and sulfur of cysteines and methionines are 3.45 and 3.32 Å, respectively, with standard deviations of 0.2 Å.[81] Considering small models with these H-bonds, we obtained after geometry optimization, using the same level of theory as for the ISC, 3.39 and 3.45 Å for the S···O distance in Cys−hydroxyl and Met−hydroxyl, respectively (see Supporting Information, Table S3.6), which are quite similar to the corresponding distances in proteins. The small discrepancies between our computed values and the reported values in protein crystal structures may be related to the different types of constraints in our models and in proteins.[34]

Table 3. Computed Redox Potentials E^{o}_{comp} of ISC Models Based on S_4 (models **1**(**a**−**e**)) and C_2 (models **2**(**a**−**c**)) Symmetry, Depending on the Number of Fe−S···H−O H-Bonds

ISC models[a]	N_H[b]	E^{o}_{comp}, mV $\varepsilon = 80$[c]	$\varepsilon = 20$[c]
1a $[Fe(SEt)_4]^{1-/2-}$ (S_4)	0	−15	−240
1b $[Fe(SEt)_3(SEtOH)]^{1-/2-}$ (C_1)	1	80	−138
1c $[Fe(SEt)_2(SEtOH)_2]^{1-/2-}$ (C_2)	2	143	−69
1d $[Fe(SEt)(SEtOH)_3]^{1-/2-}$ (C_1)	3	254	44
1e $[Fe(SEtOH)_4]^{1-/2-}$ (C_2)	4	350	144
2a $[Fe(SEt)_4]^{1-/2-}$ (C_2)	0	56	−165
2b $[Fe(SEt)_3(SEtOH)]^{1-/2-}$	1	70	−143
2c $[Fe(SEt)_2(SEtOH)_2]^{1-/2-}$ (C_2)	2	173	−36

[a] The symmetry types of the ISC models are given in parentheses. Ligand abbreviations: SEt = ethanethiol-1-ide and SEtOH = sulfanylmethanol-1-ide. [b] Number of (S···H−O) H-bonds. [c] Inside the ISC complex, the dielectric constant is unity, while for the environment, a dielectric constant of 80 corresponds to water and 20 corresponds to protein.

The redox potentials of the ISC models **1a** and **2a** are shifted positively, increasing the number of S···HO H-bonds (models **1**(**b**−**e**) and **2**(**b**−**c**)) (Table 3) depending linearly on the number of H-bonds, Figure 4. For the series of H-bonds in ISC models **1**(**a**−**e**), the linear fit yields an increase per H-bond of 90 mV in water ($\varepsilon = 80$) and 95 mV in low dielectric medium, corresponding to a protein environment ($\varepsilon = 20$). Due to the C_2 symmetry (see Figure 2), the ISC model **2a** can form only up to two H-bonds of ligands with sulfur. For this compound, the dependence of the ISC redox potentials with the number of H-bonds is evidently not linear (Figure 4). The deviation from linearity is probably due to the single H-bond in ISC model **2b** that disturbs the C_2 symmetry, which is perfectly maintained for the corresponding ISC models with none or two H-bonds. The redox potential shift due to two H-bonds is for the ISC model **2c** $\Delta E = 117$ mV (58 mV for one H-bond), which is comparable to the redox potential shift of the corresponding ISC model **1c** (with two H-bonds in S_4 symmetry yielding the shift $\Delta E = +158$ mV, see Table 3). These results indicate that the influence of H-bonds on the ISC redox potential depends on the type of symmetry of the ISC, and in the series of models **1**(**a**−**e**), the H-bonds have a stronger effect on the ISC redox potentials than in models **2**(**a**−**c**).

The experimental shifts of ISC redox potentials estimated for the formation of Fe−S···H−O H-bonds in ISC proteins range from 44 to 120 mV.[34−36] Hence, our calculated shift of 90 mV for this type of H-bond is in the range of measured values. Deviations from measured redox potentials may be due to constraints from and interactions with the protein environment.

ISC Models with Fe−S···H−N H-Bonds. Table 4 and Figure 3 contain the values of computed ISC redox potentials of models **3**(**a**−**h**) with a variable number of amide H-bonds. In Scheme 1, corresponding to model **3a,** we depicted four intramolecular H-bonds of type HB1 and HB2, involving the Cys backbone amide group and the protein backbone as in Rd, respectively. Models **3**(**b**−**h**) are variations of model **3a**, possessing similar chemical composition and dielectric boundary but involving different numbers of intramolecular H-bonds.

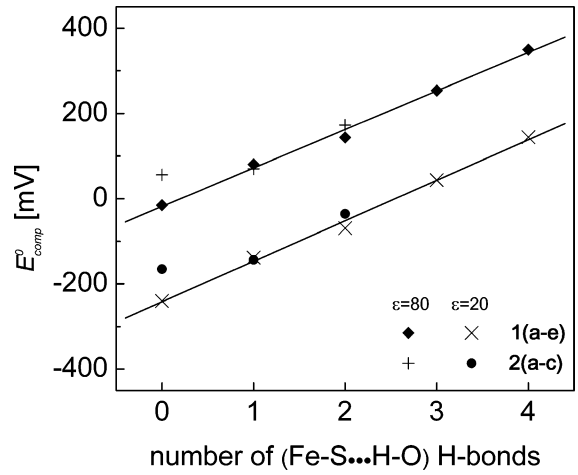

Figure 4. Calculated redox potentials as a function of the number of Fe−S···H−O H-bonds in ISC models in two dielectric environments: water- ($\varepsilon = 80$) and protein-like ($\varepsilon = 20$). Models based on S_4 symmetry allow a maximum of four H-bonds (model **1b**−**e**), while models based on C_2 symmetry allow a maximum of only two H-bonds (model **2a**−**c**).

Table 4. Computed Redox Potentials E^{o}_{comp} of ISC models **3**(**a**−**h**) with a different Number of Fe−S···H−N H-Bonds of types HB1 and HB2

ISC model[a]	N_{HB1}/N_{HB2}[b]	E^{o}_{comp}, mV $\varepsilon = 80$[c]	$\varepsilon = 20$[c]
3a $[Fe(SEt)_2(saa)_2]^{1-/2-}$	2/2	6	−161
3b $[Fe(SEt)_2(saa)(sac)]^{1-/2-}$	2/1	−22	−199
3c $[Fe(SEt)_2(sac)(sca)]^{1-/2-}$	1/2	−91	−261
3d $[Fe(SEt)_2(sac)_2]^{1-/2-}$	2/0	−100	−278
3e $[Fe(SEt)_2(sca)_2]^{1-/2-}$	0/2	−58	−232
3f $[Fe(SEt)_2(sac)(scc)]^{1-/2-}$	1/0	−171	−350
3g $[Fe(SEt)_2(sca)(scc)]^{1-/2-}$	0/1	−180	−357
3h $[Fe(SEt)_2(scc)_2]^{1-/2-}$	0/0	−238	−419

[a] For ligand abbreviations see Supporting Information, Table S2.1. [b] N_{HB1} and N_{HB2} are the numbers of H-bonds of type HB1 and HB2, respectively, Scheme 1. [c] Inside the ISC complex, the dielectric constant is unity, while for the environment, the dielectric constant of 80 corresponds to water and 20 corresponds to protein.

The S···N distances obtained in our models after geometry optimization of crystal structures vary from 3.5 to 4.3 Å (Supporting Information, Table S3.4), being in general larger than 3.3−4.0 Å observed in Rd crystal structures. Analyzing H-bonds in proteins between the NH group of the backbone and the sulfur of Cys and Met, the S···N distances are 3.61 and 3.59 Å, respectively, with standard deviations of 0.2 Å.[81] The S···N distances obtained after quantum chemical geometry optimization of Cys−amide and Met−amide models (using the same level the theory as for the ISC models) are 3.69 and 3.64 Å for Cys and Met, respectively (see Supporting Information, Table S3.6), which essentially agree with corresponding distances in proteins. Hence, constraints by the protein environment are likely not the reason for discrepancies between the computed and the measured S···N distances in ISC models and Rd. The reasons that we computed larger S···N distances in our ISC models as compared to the values in the Rd crystal structures could be the specific constraints of the ISC models not present in

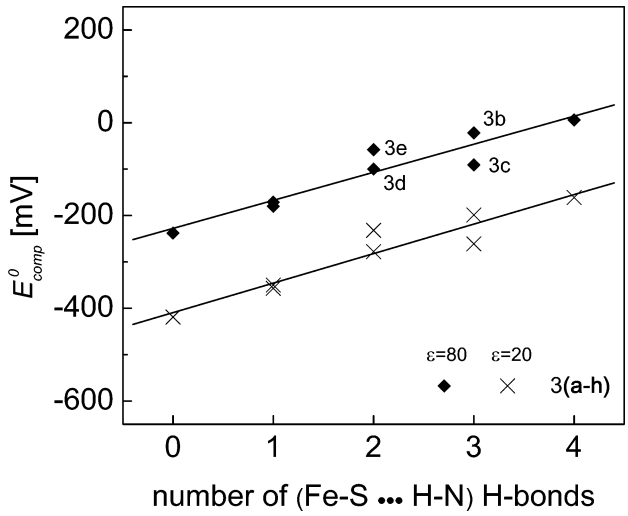

Figure 5. Calculated redox potentials as a function of the number of (S···H−N) H-bonds in the ISC models of type HB1 and HB2 (see Scheme 1) in water ($\varepsilon = 80$) and protein environments ($\varepsilon = 20$). The ISC model pairs (**3b**,**c**), (**3d**,**e**), (**3f**,**g**) possess the same number of H-bonds in different positions (see Figure 3).

the protein or the level of quantum chemical theory,[57] which may not be appropriate in the presence of iron.

The redox potentials of ISC models **3**(**a**−**h**) with S···H−N H-bonds are plotted in Figure 5. The linear fit yields a shift of the redox potential per H-bond of 60 and 65 mV in water and protein environments, respectively. This value agrees with the estimated value of 70 mV from measurements in Rieske and Rieske-type proteins.[18] From our ISC models, it is not possible to distinguish which type of H-bond (HB1 or HB2) exerts a stronger redox potential shift.

Rubredoxin Redox Potential. Model **4** is our largest ISC model (101 atoms) in this study designed to mimic the H-bond pattern in Rd. Although this model follows the orientation of the ISC and H-bonds as found in *Cp* Rd, it does not include the side chains denoted in Scheme 1. The ISC model **4** corresponds to a sequence involving only glycine (G) at two positions with an incomplete backbone (IBB) [8(G)10(G)11(IBB)41(G)43(G)44(IBB)]. It can best be compared with the *Cp* Rd mutant[29] [8(G)10(G)11(Y)41(L)-43(G)44(G)]. Although there is an experimental value of the redox potential reported for this *Cp* Rd mutant (+39 mV),[29] there is no crystal structure for this protein available. We compared model **4** in the oxidized state with the wild-type *Cp* Rd crystal structure (PDB code 1IRO), yielding a rmsd (without hydrogen atoms) of 0.577 Å. Major structural deviations of model **4** compared to the ISC in Rd are with respect to the two terminal methyl groups (black carbon atoms in Figure 1b), corresponding to the IBBs at positions 11 and 44, which are constraints in the protein. We also observed deviations in the six dihedral angles H−N−C−O, whose hydrogens are involved in the H-bonds.

Comparing the reduced and oxidized state geometries, the ISC model **4** yields an rmsd of 0.25 Å, that is comparable to 0.18 Å obtained by considering the equivalent atoms in the crystal structures of *Cp* Rd.[82] We can also compare equivalent atoms in the optimized geometries of model **4** with the *Cp* Rd crystal structures in the corresponding redox states: 1FHH (oxd) and 1FHM (red),[82] yielding an rmsd of 0.57 and 0.52 Å for the oxidized and reduced states, respectively. Major structural deviations of model **4** from the Rd crystal structures are with respect to the two terminal methyl groups (black carbon atoms in Figure 1b), corresponding to the IBBs at positions 11 and 44, which are constraints in the protein. We also observed deviations in equivalent dihedral angles H−N−C−O involving the H-bond hydrogens between the ISC model and the Rd. In the latter case, the H-bond strengths vary with the amino acid type in those positions.[33]

Table 5. Calculated Redox Potentials of ISC Model **4** in Different Dielectric Environments and Comparison with Experimental Values with Similar ISC Ligand Composition[a]

	E^0_{comp}, mV		
ISC model	$\varepsilon = 80$[b]	$\varepsilon = 20$[b]	AN[c]
4 $[Fe(saaa)_2]^{1-/2-d}$	194	57	−100
		Rd interval[e]	Rd analogue[f]
measured redox potentials		(−87, +39)	−136

[a] Model 4 possesses six amide H-bonds similar to Rd, see Scheme 1 and Figure 1b. [b] Inside the ISC complex, the dielectric constant is unity, while for the environment, the dielectric constant of 80 corresponds to water and 20 corresponds to protein. [c] AN with $\varepsilon = 37.5$. [d] For the ligand abbreviation, see Supporting Information, Table S1 [e] Rd experimental values,[29] for a complete list see Supporting Information, Table S2. [f] Synthetic peptide-based ISC model as Rd analogue.[24]

The redox potentials computed of ISC model **4** are shown in Table 5. For water ($\varepsilon = 80$), it is +194 mV, while for the protein environment ($\varepsilon = 20$), it is +57 mV. The measured redox potentials of Rd vary between −87 and +39 mV in different species of Rd[9,53,72,83,84] (see Supporting Information, Table S1.1 for a more complete list of references). Our computed ISC redox potential of model **4** is more positive, which can qualitatively be understood, since it involves only Gly residues in positions with amide H-bonds with sulfur. Experiments with *Cp* Rd mutants exhibit a redox potential that is down shifted by about 70 mV,[29,31] mutating from Val to Gly. Interestingly, our computed ISC redox potential +57 mV is close to +39 mV measured for a *Cp* Rd mutant[29] whose sequence [8(G)10(G)11(Y)41(L)43(G)44(G)] involved in ISC H-bonds is closest to model **4**.

We also computed the redox potential of model **4** in AN obtaining −100 mV, which can be compared with the redox potential −136 mV[24] measured in AN for a synthetic peptide-based ISC model with the sequence [8(L)10(G)11(Fp)-41(G)43(G)44(Fp)] (Fp is a Phe-like compound[24]) similar in chemical composition to model **4**. Figure 6 shows the dependence of the computed redox potential of ISC model **4** for different dielectric constants together with the range of measured Rd redox potentials, the range of dielectric constants used to describe an implicit protein model, and the computed and measured redox potentials of the above synthetic ISC model and model **4** in AN.

Our Rd-like ISC model **4** is at the limit of what we can compute at present to evaluate absolute values of redox potentials for ISC models fully quantum chemically. To study the Rd protein in more detail with quantum chemical computations requires more efficient methods like QM/MM[85,86]

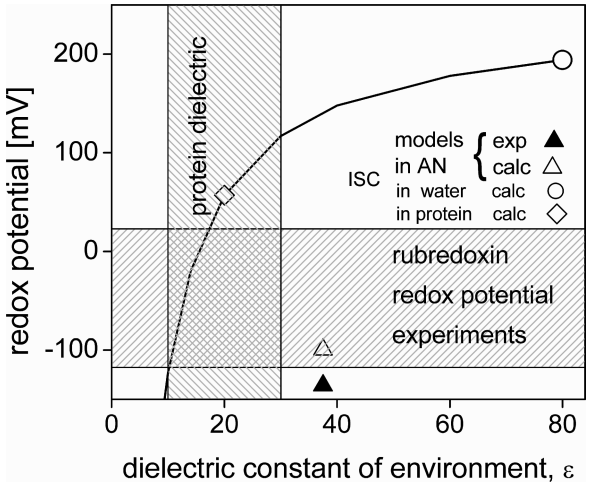

Figure 6. Dependence of the computed redox potential of ISC model **4** as a function of the environmental dielectric constant. The measured Rd redox potentials are within the shaded horizontal regime. The dielectric constants used for implicit protein models are in the shaded vertical regime. The computed redox potentials of ISC model **4** in water and AN are given by the open circle and triangle, respectively. The experimental redox potential for a similar peptide-based ISC in AN is given as the closed triangle.[24] The computed redox potential of model **4** with $\varepsilon = 20$, corresponding to a protein environment is given as the open diamond.

that describe the more distant parts of the complete protein classically and can, therefore, consider also different conformations. However, this approach is beyond the scope of this study. Alternatively, we can use a purely electrostatic approach, which also allows to consider the influence of protonation pattern and hydrogen atom flexibility[87] on the redox potentials of the protein cofactors[78] and the aspects of coupling between electron and proton transfer processess.[88−90] This will be subject of future work.

Factors Shifting Redox Potential in ISC Models. The first factor we discussed was the variation in conformational symmetry between S_4 and C_2. The computed redox potential shift (from model **1a** to **2a**) was 71 mV in water ($\varepsilon = 80$), while for AN ($\varepsilon = 37.5$), the shift was 211 mV. The second factor shifting the ISC redox potential is the number and the type of H-bonds with ISC sulfurs. As we have demonstrated, the shift per H-bond could vary from 65 to 95 mV depending on the type and the geometrical constraints. H-bonds stabilize the negative charge of the ISC in Rd.

The last factor we consider is due to dielectric environment. Comparing at $\varepsilon = 80$, the small ISC model **2a** with the larger ISC model **3h**, both of them without H-bonds, the redox potential decreases from +56 to −238 mV. This demonstrates how a low dielectric can down-shift the ISC redox potential (about 294 mV in this case) when one places a small ISC model in a protein-like environment. A similar down-shift of 221 mV is computed when model **2a** is placed in a low dielectric with $\varepsilon = 20$. The qualitative agreement suggests that the use of $\varepsilon = 20$ for the implicit protein model is appropriate. The results obtained for our ISC models show the importance of the dielectric environment in tuning the ISC redox potentials and how the degree of solvent exposure of ISC can affect the redox potential.

Inside the protein, these factors may vary in strength and may be coupled. For example, the experiments performed to measure the influence of H-bond strength by means of side chain mutations in rubredoxin mutants[30,33] affect not only the strength of ISC H-bonds but change also the electrostatic volume of the amino acid side chains involved in H-bonds, thus, decreasing the capacity of charge transfer from H-bonds to neighboring atoms.[82,91] Both effects change the redox potential and may act in opposite directions. Hence, in our study, we separated the factors changing ISC redox potentials, making it easier to understand the magnitude and the direction of redox potential shifts depending on the conformations, the H-bonds, and the dielectric environment, all important for ISC proteins.

Conclusions

Using the B4(XQ3)LYP approach, we calculated absolute redox potentials of 17 ISC models related to the ISC in Rd in different media, which are water, AN, and protein-like environment. In AN, the ISC redox potentials are very negative being below −800 mV for the most elementary ISC model with S_4 symmetry, while in water and protein environment, the redox potentials are close to zero. Part of this enormous upshift is due to a change in symmetry from S_4 to C_2, yielding about +200 mV in AN. The remaining part of the redox potential upshift of +600 mV is due to the difference between the aprotic environment provided by AN and the protic environment provided by water. In an implicit solvent model for water, using continuum electrostatics, the energetics of H-bonds are described implicitly by surface charges at the electrostatic boundaries. The ISC models of this study that mimic the protein environment consider polar hydrogen atom contacts to form explicit H-bonds.

The redox potentials computed in the present study agree with available measured values in the range of 50 mV in analogy to the agreement found for the large number of redox potentials, which were computed for transition metal complexes before.[1] This degree of accuracy could only be achieved with the modified B4(XQ3)LYP functional in DFT combined with a post-SCF correction followed by continuum electrostatics to evaluate solvation energies. In this connection, also electrostatic energies were optimized by choosing appropriate atomic radii. Using of the same electrostatics in combination with the B3LYP functional results in an rmsd of 183 mV,[1] comparable with 170 mV reported for calculated redox potentials of 270 different organic compounds.[60]

We explored the influence of two different H-bond partners, Fe−S···H−O and Fe−S···H−N on the ISC redox potentials. We found that in aqueous solution ($\varepsilon = 80$) one Fe−S···H−O H-bond up-shifts the ISC redox potential by 58 mV for the C_2 symmetry and by 90 mV for the S_4 symmetry. In a low dielectric environment ($\varepsilon = 20$) as in proteins, the computed upshift of the ISC redox potential is expected to be 77 mV for a single

Fe−S···H−N H-bond correlating well with the experimental estimate of 70 mV in Rieske proteins.[18] The H-bond influence on ISC redox potentials is larger for Fe−S···H−O than for Fe−S···H−N H-bonds due to the higher polarity of OH groups compared to NH groups in the ISC models of this study. We calculated the redox potential for a model complex that mimics the ISC inside the protein environment and obtained good agreement with experimental values of a Rd-like ISC and an ISC in Rd. This practically quantitative agreement between the computation and the experiment allows to understand the redox potential shift between small ISC models and ISC in proteins, which depends on three factors: the change in conformation, (from symmetry S_4 to C_2, shifting the redox potential by 71 mV), the number of H-bonds (about 60 mV for a single Fe−S···H−N and 90 mV for Fe−S···H−O H-bond) and the degree of solvent exposure (about 200 mV down-shift going from high to low dielectric environment).

Acknowledgment. We thank Dr. Hiroshi Ishikita for useful discussions, and we are grateful for financial support from CONACyT, DAAD, and the Deutsche Forschungsgemeinschaft SFB 498 project A5.

Note Added after ASAP Publication. This paper was published ASAP on September 16, 2009. A line describing eq 1 in the Materials and Methods section was corrected. The revised paper was reposted on September 28, 2009.

Supporting Information Available: Listings of Rd pdb information, H-bonds geometrical parameters of ISC models and respective atomic partial charges, charge distribution plot, computed energy tables, and H-bond energies. This material is available free of charge via the Internet at http://pubs.acs.org.

References

(1) Galstyan, A. S.; Knapp, E. W. *J. Comput. Chem.* **2009**, *30*, 203–211.

(2) Hall, D. O.; Cammack, R.; Rao, K. K. *Origins Life Evol. Biosphere* **1974**, *5*, 363–386.

(3) Holm, R. H.; Kennepohl, P.; Solomon, E. I. *Chem. Rev.* **1996**, *96*, 2239–2314.

(4) Beinert, H.; Holm, R. H.; Münck, E. *Science* **1997**, *277*, 653.

(5) Imsande, J. *Plant Physiol. Biochem.* **1999**, *37*, 87–97.

(6) Beinert, H. *J. Biol. Inorg. Chem.* **2000**, *5*, 2–15.

(7) Langen, R.; Jensen, G. M.; Jacob, U.; Stephens, P. J.; Warshel, A. *J. Biol. Chem.* **1992**, *267*, 25625–25627.

(8) Bertini, I.; Ciurli, S.; Luchinat, C. In *Iron-Sulfur Proteins Perovskites*; Springer-Verlag: Berlin, Germany, 1995; Vol. 83, p 1−53.

(9) Stephens, P. J.; Jollie, D. R.; Warshel, A. *Chem. Rev.* **1996**, *96*, 2491–2531.

(10) Eidsness, M. K.; Burden, A. E.; Richie, K. A.; Kurtz, D. M.; Scott, R. A.; Smith, E. T.; Ichiye, T.; Beard, B.; Min, T.; Kang, C. *Biochemistry* **1999**, *38*, 14803.

(11) Maelia, L. E.; Millar, M.; Koch, S. A. *Inorg. Chem.* **1992**, *31*, 4594–4600.

(12) Johnson, R. E.; Papaefthymiou, G. C.; Frankel, R. B.; Holm, R. H. *J. Am. Chem. Soc.* **1983**, *105*, 7280–7287.

(13) Backes, G.; Yoshiki, M.; Loehr, T. M.; Meyer, T. E.; Cusanovich, M. A.; Sweeney, W. V.; Adman, E. T.; Sanders-Loehr, J. *J. Am. Chem. Soc.* **1991**, *113*, 2055–2064.

(14) Zheng, H.; Kellog, S. J.; Erickson, A. E.; Dubauskie, N. A.; Smith, E. T. *J. Biol. Inorg. Chem.* **2003**, *8*, 12–18.

(15) Dey, A.; Jenney, F. E., Jr.; Adams, M. W. W.; Babini, E.; Takahashi, Y.; Fukuyama, K.; Hodgson, K. O.; Hedman, B.; Solomon, E. I. *Science* **2007**, *318*, 1464.

(16) Adman, E. T.; Watenpaugh, K. D.; Jensen, L. H. *P. Natl. Acad. Sci. U.S.A.* **1975**, *72*, 4854–4858.

(17) Rose, K.; Shadle, S. E.; Eidsness, M. K.; Jr., D. M. K.; Scott, R. A.; Hedman, B.; Hodgson, K. O.; Solomon, E. I. *J. Am. Chem. Soc.* **1998**, *120*, 10743–10747.

(18) Hunsicker-Wang, L. M.; Heine, A.; Chen, Y.; Luna, E. P.; Todaro, T.; Fee, J. A. *Biochemistry* **2003**, *42*, 7303–7317.

(19) Solomon, E. I.; Gorelsky, S. I.; Dey, A. *J. Comput. Chem.* **2006**, *27*, 1415–1428.

(20) Carter, C. W. J. *J. Biol. Chem.* **1977**, *252*, 7802–7811.

(21) Low, D. W.; Hill, M. G. *J. Am. Chem. Soc.* **2000**, *122*, 11039–11040.

(22) Nakata, M.; Ueyama, N.; Fuji, M.-A.; Nakamura, A.; Wada, K.; Matsubara, H. *Biochim. Biophys. Acta* **1984**, *788*, 306–312.

(23) Ueyama, N.; Nakata, M.; Fuji, M. A.; Terakawa, T.; Nakamura, A. *Inorg. Chem.* **1985**, *24*, 2190–2196.

(24) Sun, Y.-W.; Ueyama, N.; Nakamura, A. *Inorg. Chem.* **1991**, *30*, 4026–4031.

(25) Walters, M. A.; Dewan, J. C.; Min, C.; Pinto, S. *Inorg. Chem.* **1991**, *30*, 2656–2662.

(26) Huang, J.; Ostrander, R. L.; Rheingold, A. L.; Walters, M. A. *Inorg. Chem.* **1995**, *34*, 1090–1093.

(27) Chung, W. P.; Dewan, J. C.; Turkerman, M.; Walters, M. A. *Inorg. Chim. Acta* **1999**, *291*, 388–394.

(28) Walters, M. A.; Roche, C. L.; Rheingold, A. L.; Kassel, S. W. *Inorg. Chem.* **2005**, *44*, 3777–3779.

(29) Xiao, Z.; Maher, M. J.; Cross, M.; Bond, C. S.; Guss, J. M.; Wedd, A. G. *J. Biol. Inorg. Chem.* **2000**, *5*.

(30) Lin, I. J.; Gebel, E. B.; Machonkin, T. E.; Westler, W. M.; Markley, J. L. *J. Am. Chem. Soc.* **2003**, *125*, 1464–1465.

(31) Park, I. Y.; Eidsness, M. K.; Lin, I. J.; Gebel, E. B.; Youn, B.; Harley, J. L.; Machonkin, E. E.; Frederick, R. O.; Markley, J. L.; Smith, E. T.; Ichiye, T.; Kang, C. *Proteins* **2004**, *57*, 618.

(32) Park, I. Y.; Youn, B.; Harley, J. L.; Eidsness, M. K.; Smith, E.; Ichiye, T.; Kang, C. *J. Biol. Inorg. Chem.* **2004**, *9*, 423.

(33) Lin, I. J.; Gebel, E. B.; Machonkin, T. E.; Westler, W. M.; Markley, J. L. *Proc. Natl. Acad. Sci. U.S.A.* **2005**, *102*, 14581–14586.

(34) Bönisch, H.; L., S. C.; P., B.; Ladenstein, R. *J. Biol. Inorg. Chem.* **2007**, *12*, 1163–1171.

(35) Schröter, T.; Hatzfeld, O. M.; Gemeinhardt, S.; Korn, M.; Friedrich, T.; Ludwig, B.; Link, T. A. *Eur. J. Biochem.* **1998**, *255*, 100–106.

(36) Denke, E.; Merbitz-Zahradnik, T.; Hatzfeld, O. M.; Snyder, C. H.; Link, T. A.; Trumpower, B. L. *J. Biol. Chem.* **1998**, *273*, 9085–9093.

(37) Ayhan, M.; Xiao, Z.; Lavery, M. J.; Hamer, A. M.; Nugent, K. W.; Scrofani, S. D. B.; Guss, M.; Wedd, A. G. *Inorg. Chem.* **1996**, *35*, 5902–5911.

(38) Dolan, E. A.; Yelle, R. B.; Beck, B. W.; Fischer, J. T.; Ichiye, T. *Biophys. J.* **2004**, *86*, 2030–2036.

(39) Mouesca, J. M.; Chen, J. L.; Noodleman, L.; Bashford, D.; Case, D. A. *J. Am. Chem. Soc.* **1994**, *116*, 11898–11914.

(40) Li, J.; Nelson, M. R.; Peng, C. Y.; Bashford, D.; Noodleman, L. *J. Phys. Chem. A* **1998**, *102*, 6311–6324.

(41) Ullmann, G. M.; Noodleman, L.; Case, D. A. *J. Biol. Inorg. Chem.* **2002**, *7*, 623–639.

(42) Yelle, R. B.; Park, N.-S.; Ichiye, T. *Proteins* **1995**, *22*, 154–167.

(43) Ergenekan, C. E.; Thomas, D.; Fischer, J. T.; Tan, M.-L.; Eidsness, M. K. *Biophys. J.* **2003**, *85*, 2818–2829.

(44) Tan, M.-L.; Kang, C.; Ichiye, T. *Proteins* **2006**, *62*, 708–714.

(45) Sulpizi, M.; Raugei, S.; Vondele, J. V.; Carloni, P.; Sprik, M. *J. Phys. Chem. B* **2007**, *111*, 3969–3976.

(46) Schmidt am Busch, M.; Knapp, E. W. *J. Am. Chem. Soc.* **2005**, *127* (45), 15730–15737.

(47) Curtiss, L. A.; Redfern, P. C.; Raghavachari, K.; Rassolov, V.; Pople, J. A. *J. Chem. Phys.* **1999**, *110*, 4703–4709.

(48) Noodleman, L.; Norman, J. G., Jr.; Osborne, J. H.; Aizman, A.; Case, D. A. *J. Am. Chem. Soc.* **1985**, *107*, 3418–3426.

(49) Noodleman, L.; Lovell, T.; Liu, T.; Himo, F.; Torres, R. A. *Curr. Opin. Chem. Biol.* **2002**, *6*, 259–273.

(50) Torres, R. A.; Lovell, T.; Noodleman, L.; Case, D. A. *J. Am. Chem. Soc.* **2003**, *125*, 1923–1936.

(51) Noodleman, L.; Han, W. G. *J. Biol. Inorg. Chem.* **2006**, *11*, 674–694.

(52) Solomon, E. I.; Xie, X.; Dey, A. *Chem. Soc. Rev.* **2008**, *37*, 623–638.

(53) Dauter, Z.; Wilson, K. S.; Sieker, L. C.; Moulis, J.-M.; Meyer, J. *Proc. Natl. Acad. Sci. U.S.A.* **1996**, *93*, 8836.

(54) Schmidt am Busch, M.; Knapp, E. W. *ChemPhysChem* **2004**, *5*, 1513–1522.

(55) Koch, S. A.; Maelia, L. E.; Millar, M. *J. Am. Chem. Soc.* **1983**, *105*, 5944–5945.

(56) Millar, M.; Lee, J. F.; O'Sullivan, T.; Koch, S. A.; Fikar, R. *Inorg. Chim. Acta* **1996**, *243*, 333–343.

(57) Szilagyi, R. K.; Winslow, M. A. *J. Comput. Chem.* **2006**, *27*, 1385–1397.

(58) Koerner, J. B.; Ichiye, T. *J. Phys. Chem. B* **1997**, *101*, 3633–3643.

(59) Yang, X.; Niu, S.; Ichiye, T.; Wang, L. S. *J. Am. Chem. Soc.* **2004**, *126*, 15790–15794.

(60) Fu, Y.; Liu, L.; Yu, H.-Z.; Wang, Y.-M.; Guo, Q.-X. *J. Am. Chem. Soc.* **2005**, *127*, 7227–7234.

(61) Reiss, H.; Heller, A. *J. Phys. Chem.* **1985**, *89*, 4207–4213.

(62) Trasatti, S. *Pure Appl. Chem.* **1986**, *58*, 955–966.

(63) Lewis, A.; Bumpus, J. A.; Truhlar, D. G.; Cramer, C. J. *J. Chem. Educ.* **2004**, *81*, 596–604.

(64) Tissandier, M. D.; Cowen, K. A.; Feng, W. Y.; Gundlach, E.; Cohen, M. H.; Earhart, A. D.; Coe, J. V.; Tuttle, T. R. *J. Phys. Chem. A* **1998**, *102*, 7787–7794.

(65) Slater, J. C. *Quantum Theory of Molecules and Solids*; McGraw-Hill: New York, 1974.

(66) Vosko, S. H.; Wilk, L.; Nusair, M. *Can. J. Phys.* **1980**, *58*, 1200–1211.

(67) Becke, A. D. *Phys. Rev. A: At., Mol., Opt. Phys.* **1988**, *38*, 3098–3100.

(68) Lee, C.; Yang, W.; Paar, R. G. *Phys. Rev. B: Solid State* **1988**, *37*, 785–789.

(69) Becke, A. D. *J. Chem. Phys.* **1993**, *98*, 5648–5652.

(70) Hay, P. J.; Wadt, W. R. *J. Phys. Chem.* **1985**, *82*, 299–310.

(71) *Jaguar, 5.5*; Schroedinger, L.L.C.: Portland, OR, 1991−2003.

(72) Adams, M. W. *Adv. Inorg. Chem.* **1992**, *38*, 341–396.

(73) Bayly, C.; Cieplak, P.; Cornell, W.; Kollman, P. *J. Phys. Chem.* **1993**, *97*, 10269–10280.

(74) Cornell, W.; Cieplak, P.; Bayly, C.; Kollman, P. *J. Am. Chem. Soc.* **1993**, *115*, 9620–9631.

(75) Gilson, M.; Honig, B. *Biopolymers* **1986**, *25*, 2097–2119.

(76) Schutz, C. N.; Warshel, A. *Proteins* **2001**, *44*, 400–417.

(77) Warshel, A.; Sharma, P. K.; Kato, M.; Parson, W. W. *Biochim. Biophys. Acta* **2006**, *1764*, 1647–1676.

(78) Ullmann, G. M.; Knapp, E. W. *Eur. Biophys. J.* **1999**, *28*, 533–551.

(79) Bashford, D.; Gerwert, K. *J. Mol. Biol.* **1992**, *224*, 473–486.

(80) Bashford, D.; Karplus, M. *J. Phys. Chem.* **1991**, *95*, 9557–9561.

(81) Zhou, P.; Tian, F.; Lv, F.; Shang, Z. *Proteins: Structure, Function, and Bioinformatics* **2009**, *76*, 151–163.

(82) Min, T.; Ergenekan, C. E.; Eidsness, M. K.; Ichiye, T.; Kang, C. *Protein Sci.* **2001**, *10*, 613.

(83) Gillès de Pélichy, L. D.; Smith, E. T. *Biochemistry* **1999**, *38*, 7874–7880.

(84) Day, M. W.; Hsu, B. T.; Joshuator, L.; Park, J. B.; Zhou, Z. H.; Adams, M. W.; Rees, D. C. *Protein Sci.* **1992**, *1*, 1494.

(85) Elstner, M.; Thomas, F.; Suhai, S. *THEOCHEM* **2003**, *632*, 29–41.

(86) Maseras, F.; Morokuma, L. *J. Comput. Chem.* **1995**, *16*, 1170–1179.

(87) Kieseritzky, G.; Knapp, E. W. *Proteins: Structure, Function and Bioinformatics* **2008**, *71*, 1335–1348.

(88) Rabenstein, B.; Knapp, E. W. *Biophys. J.* **2001**, *80*, 1141–1150.

(89) Baptista, A. M.; Martel, P. J.; Soares, C. M. *Biophys. J.* **1999**, *76*, 2978–2998.

(90) Onufriev, A.; Case, D. A.; Ullmann, G. M. *Biochemistry* **2001**, *40*, 3413–3419.

(91) Gutman, V.; Resch, G.; Linert, W. *Coord. Chem. Rev.* **1982**, *43*, 133–164.

CT900328C